FULL PAPER

Dalton
www.rsc.org/dalton

Solid state coordination chemistry: secondary metal–ligand influences on the structures of vanadium oxides. Hydrothermal syntheses and structures of $[Zn(tpytrz)_2V_2O_6]$, $[Zn_3(tpytrz)_2(H_2O)_2V_6O_{18}]\cdot 6H_2O$ and $[Cu_3(tpytrz)_2(H_2O)_2V_8O_{23}]\cdot 3H_2O$ (tpytrz = 2,4,6-tri(4-pyridyl)-1,3,5-triazine) †

Randy S. Rarig, Jr. and Jon Zubieta *
Department of Chemistry, Syracuse University, Syracuse, NY 13244, USA

Received 16th December 2002, Accepted 12th March 2003
First published as an Advance Article on the web 2nd April 2003

The hydrothermal reactions of $Zn(SO_4)\cdot 5H_2O$, V_2O_5 and 2,4,6-tri(4-pyridyl)-1,3,5-triazine (tpytrz) yield $[Zn(tpytrz)_2V_2O_6]$ (**1**) at pH 6.5 and $[Zn_3(tpytrz)_3(H_2O)_2V_6O_{18}]\cdot 6H_2O$ (**2**·6H_2O) at pH 3.5. Substitution of Cu(II) as the secondary metal in the reaction of $Cu(SO_4)\cdot 5H_2O$, V_2O_5 and tpytrz yields $[Cu_3(tpytrz)_2(H_2O)_2V_8O_{23}]\cdot 3H_2O$ (**3**·3H_2O). The structure of **1** consists of a bimetallic oxide layer, decorated on both surfaces by monodentate tpytrz groups. The structure of **2** is three-dimensional and constructed from a 3-D bimetallic oxide framework with the organic subunit entrained within larger channels in the oxide scaffolding. While the structure of **3** is grossly similar to that of **2**, the different coordination preferences of Zn(II) and Cu(II) are manifested in the detailed structural features. Thus, while the vanadate substructure of **2** is one-dimensional, that of **3** is two-dimensional. Similarly, **2** exhibits both tetrahedral and octahedral secondary metal sites, while **3** possesses only '4 + 2' axially distorted Cu(II) sites.

The inorganic oxides are ubiquitous materials possessing an extensive compositional range and structural diversity, characteristics reflected in useful physical properties giving rise to applications in sorption, catalysis, photonics and microelectronics.[1–4] The fundamental and practical importance of oxides has engendered considerable interest in the synthesis of new materials of enhanced structural complexity and potential functionality.[5,6] A common approach to the design of novel oxide materials exploits organic building blocks to provide additional structural diversity and some control of the oxide microstructure.[7] The resulting organic–inorganic hybrid oxide combines the unique characteristics of the components in novel solid phases with composite or even unique properties.[8]

Our strategy for the design of new molybdenum oxide materials introduced the organic component as a ligand to a secondary transition metal center to form bimetallic, organically templated hybrids.[9–26] The structure of the composite reflects not only the geometric constraints of the ligand but also the coordination preferences of the secondary metal which may be spatially transmitted through appropriate tethering organic subunits. This design principle was manifested in a series of three-dimensional secondary metal–ligand molybdate materials $[M'(tpytrz)_2Mo_4O_{13}]$ (M′ = Fe, Co, Ni, Zn), $[Ni(tpytrz)Mo_2O_7]$ and $[Zn_2(tpytrz)Mo_2O_8]$, where tpytrz is 2,4,6-tri(4-pyridyl)-1,3,5-triazine.[26] The architectures of these oxides exhibit a recurring structural theme of organic–inorganic hybrid materials: inorganic networks alternating with organic domains as shown in Scheme 1.[27,28] Consequently, the structures may be described as bimetallic oxide layers tethered through the tpytrz ligands acting as dipodal buttresses.

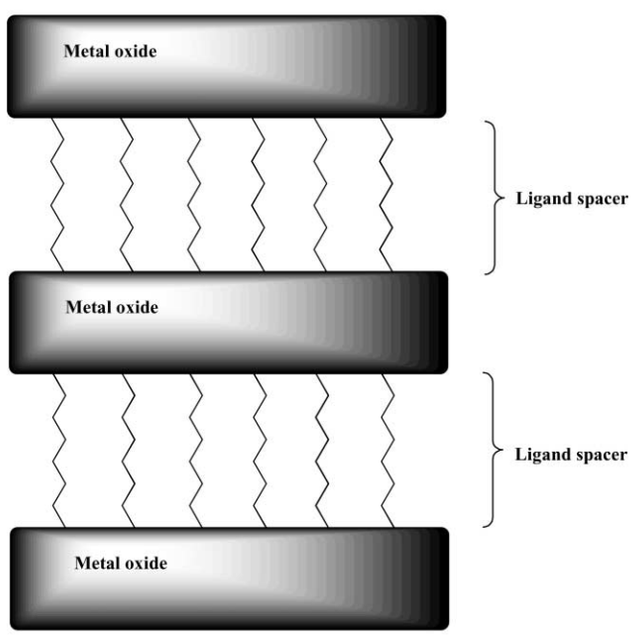

Scheme 1

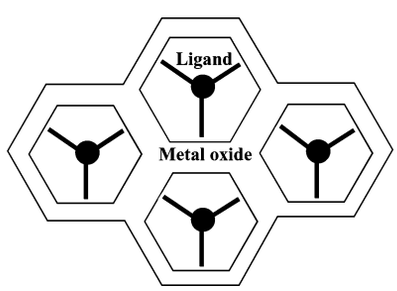

Scheme 2

While the architecture of Scheme 1 is prototypical, an alternative modality of ligand incorporation may be entertained, one in which the organic serves as a template about which the metal oxide substructure is organized. As shown in Scheme 2, this mode of ligand entrainment within the oxide scaffolding is reminiscent of the use of organoammonium cations in the design of zeolites. However, in this latter case, the cationic organic subunit functions in a charge-compensating and space-filling role, while the mode of ligand incorporation in Scheme 2 involves direct coordination to the metal. While the molybdate family of hybrids with tpytrz exhibited the structural type of Scheme 1 exclusively, we have found that the vanadium oxide chemistry is more structurally diverse, as represented by

† Electronic supplementary information (ESI) available: colour versions of Fig. 1–3. See http://www.rsc.org/suppdata/dt/b2/b212458k/

DOI: 10.1039/b212458k

Table 1 Summary of crystallographic data for the structures of $[Zn(tpytrz)_2V_2O_6]$ (**1**), $[Zn_3(tpytrz)_2(H_2O)_2V_6O_{18}]\cdot 6H_2O$ (**2**·$6H_2O$), and $[Cu_3(tpytrz)_2(H_2O)_2V_8O_{23}]\cdot 3H_2O$ (**3**·$3H_2O$)

	1	**2**	**3**
Empirical formula	$C_{18}H_{12}N_6O_3VZn_{0.5}$	$C_{18}H_{20}N_6O_{13}V_3Zn_{1.5}$	$C_{18}H_{17}Cu_{1.5}N_6O_{14}V_4$
M	443.96	779.28	840.45
Crystal system	Orthorhombic	Monoclinic	Orthorhombic
Space group	*Fdd*2	$P2_1/c$	*Pbcn*
a/Å	15.825(1)	7.8393(3)	14.368(3)
b/Å	81.248(6)	22.8107(9)	25.739(5)
c/Å	5.3089(4)	15.1124(6)	14.813(3)
α/°	90.	90.	90.
β/°	90.	102.363(1)	90.
γ/°	90.	90.	90.
V/Å^3	6825.9(9)	2639.74(2)	5478.4(2)
Z	16	4	8
D_{calc}/g cm^{-3}	1.728	1.961	2.038
μ/cm^{-1}	13.03	24.47	25.35
$R1$ [a]	0.0435	0.0594	0.0863
$wR2$ [b]	0.1026	0.1461	0.1435

[a] $R1 = \Sigma||F_o| - |F_c||/\Sigma|F_o|$. [b] $wR2 = \{\Sigma[w(F_o^2 - F_c^2)^2/\Sigma w(F_o^2)^2]\}^{1/2}$. For all data.

the two-dimensional $[Zn(tpytrz)_2V_2O_6]$ (**1**) and the three-dimensional $[Zn_3(tpytrz)_2(H_2O)_2V_6O_{18}]\cdot 6H_2O$ (**2**·$6H_2O$) and $[Cu_3(tpytrz)_2(H_2O)_2V_8O_{23}]\cdot 3H_2O$ (**3**·$3H_2O$) which exhibit structures based on the ligand incorporation pattern of Scheme 2.

Experimental

Syntheses and spectroscopy

Syntheses were carried out in Parr acid digestion bombs with 23 ml poly(tetrafluoroethylene) liners. All starting materials, with the exception of 2,4,6-tri(4-pyridyl)-1,3,5-trazine, $(C_5H_4N)_3C_3N_3$, were purchased from Aldrich and used without further purification. 2,4,6-Tri(4-pyridyl)-1,3,5-triazine was prepared according to the literature method.[29] Water was distilled above 0.3 MΩ in-house using a Barnstead model 525 Biopure distilled water center. Infrared spectra were obtained on a Perkin-Elmer 1600 series FTIR spectrometer.

Preparation of $[Zn(tpytrz)_2V_2O_6]$ (1). A solution of $Zn(SO_4)\cdot 5H_2O$ (0.14 g, 0.55 mmol), V_2O_5 (0.061 g, 0.33 mmol), 2,4,6-tri(4-pyridyl)-1,3,5-triazine (0.069 g, 0.22 mmol) and H_2O (10 g, 0.55 mol) in the mole ratio 2.5 : 1.5 : 1 : 2500 was heated for 72 h at 200 °C. Yellow crystals of **1** were isolated in 60% yield. Anal. Calcd. for $C_{18}H_{12}N_6O_3VZn_{0.5}$: C, 48.7; H, 2.70; N, 18.9. Found: C, 48.5; H, 2.63; N, 18.7%.

Preparation of $[Zn_3(tpytrz)_2(H_2O)_2V_6O_{18}]\cdot 6H_2O$ (2·$6H_2O$). A solution of $Zn(SO_4)\cdot 5H_2O$ (0.14 g, 0.55 mmol), V_2O_5 (0.061 g, 0.33 mmol), tpytrz (0.069 g, 0.22 mmol) and H_2O (10 g, 0.55 mol) and sufficient 1 molar HCl to adjust the pH to 3.5 was heated for 72 h at 200 °C. Yellow crystals of **2**·$6H_2O$ were collected in 50% yield. Anal. Calcd. for $C_{18}H_{20}N_6O_{13}V_3Zn_{1.5}$: C, 27.7; H, 2.57; N, 10.8. Found: C, 27.8; H, 2.71; N, 10.6%.

Preparation of $[Cu_3(tpytrz)_2(H_2O)_2V_8O_{23}]\cdot 3H_2O$ (3·$3H_2O$). A solution of $Cu(SO_4)\cdot 5H_2O$ (0.14 g, 0.55 mmol), V_2O_5 (0.061 g, 0.33 mmol), tpytrz (0.069 g, 0.22 mmol) and H_2O (10 g, 0.55 mol) in the mole ratio 2.5 : 1.5 : 1 : 2500 was heated at 200 °C for 72 h to give green crystals of **3**·$3H_2O$ in 30% yield. Anal. Calcd. for $C_{18}H_{17}Cu_{1.5}N_6O_{14}V_4$: C, 25.7; H, 2.02; N, 9.99. Found: C, 25.6; H, 1.84; N, 10.1%.

X-Ray crystallography

Crystallographic data for all compounds were collected with a Bruker P4 diffractometer equipped with a SMART CCD system.[30] and using Mo-Kα radiation (λ = 0.71073 Å). The data were collected at 90 K and corrected for Lorentz and polarization effects.[31] Absorption corrections were made using SADABS.[32] The structure solutions and refinements were carried out using the SHELXTL[33] crystallographic software package. The structures were solved using direct methods, and all of the non-hydrogen atoms were located from the initial solution. After locating all of the non-hydrogen atoms in each structure; the model was refined against F^2, initially using isotropic then anisotropic thermal displacement parameters, until the final value of Δ/σ_{max} was less than 0.001. Hydrogen atoms were located at calculated positions and included in the final cycles of refinement using a riding model. Crystal data for **1**–**3** are summarized in Table 1. Selected bond lengths and angles for compounds **1**–**3** are collected in Tables 2–4, respectively.

CCDC reference numbers 198637–198639.

See http://www.rsc.org/suppdata/dt/b2/b212458k/ for crystallographic data in CIF or other electronic format.

Results and discussion

Syntheses and structures

The use of hydrothermal conditions of synthesis allows isolation of metastable phases, rather than dense phase oxides, while avoiding thermal decomposition of the organic component.[34–36] It is also noteworthy that the differential solubilities of the organic and inorganic constituents do not pose a problem under such conditions. The reaction of $Zn(SO_4)\cdot 5H_2O$, V_2O_5 and 2,4,6-tri(4-pyridyl)-1,3,5-triazine (tpytrz) at pH 6.5–7.0 yielded $[Zn(tpytrz)_2V_2O_6]$ (**1**), as yellow crystals in good yield. Since the critical dependence of compound composition on pH of the hydrothermal reaction medium is well documented, the reaction of Zn(II) with V_2O_5 and tpytrz at pH 3.5 was carried out, yielding $[Zn_3(tpytrz)_2(H_2O)_2V_6O_{18}]\cdot 6H_2O$ (**2**·$6H_2O$). In order to assess the structural consequences of introducing a secondary metal with different coordination preferences, the reaction of Cu(II) with V_2O_5 and tpytrz was also explored. The material $[Cu_3(tpytrz)_2(H_2O)V_8O_{23}]\cdot 3H_2O$ (**3**·$3H_2O$) was isolated as green crystals.

The infrared spectra of **1**–**3** exhibited strong bands in the 790–940 cm^{-1} range, attributed to ν(V=O), ν(V–O–V) and ν(M′–O–V). A group of four bands in the 1000 to 1580 cm^{-1} region is characteristic of the tpytrz ligand.

As shown in Fig. 1, the structure of $[Zn(tpytrz)_2V_2O_6]$ (**1**) consists of a bimetallic oxide layer $\{ZnV_2O_6\}$ decorated on both surfaces by tpytrz ligands. The oxide network is constructed from $\{VO_3\}_n^{2n-}$ chains linked through $\{ZnN_2O_2\}$ tetrahedra. Each $\{VO_4\}$ tetrahedron of the vanadate chain shares two corners with adjacent vanadate tetrahedra of the chain and uses a third corner to link to a zinc tetrahedron. The fourth

Table 2 Selected bond lengths [Å] and angles [°] for $[Zn(tpytrz)_2V_2O_6]$ (**1**)

Zn(1)–O(1)	1.913(2)
Zn(1)–O(1)#1	1.913(2)
Zn(1)–N(1)	2.038(2)
Zn(1)–N(1)#1	2.038(2)
V(1)–O(3)	1.606(2)
V(1)–O(1)	1.683(2)
V(1)–O(2)	1.784(2)
V(1)–O(2)#2	1.794(2)
O(1)–Zn(1)–O(1)#1	118.5(1)
O(1)–Zn(1)–N(1)	110.37(8)
O(1)#1–Zn(1)–N(1)	105.16(7)
O(1)–Zn(1)–N(1)#1	105.16(7)
O(1)#1–Zn(1)–N(1)#1	110.37(8)
N(1)–Zn(1)–N(1)#1	106.8(1)
O(3)–V(1)–O(1)	109.8(1)
O(3)–V(1)–O(2)	109.0(1)
O(1)–V(1)–O(2)	110.4(1)
O(3)–V(1)–O(2)#2	109.1(1)
O(1)–V(1)–O(2)#2	110.65(9)
O(2)–V(1)–O(2)#2	107.86(5)
V(1)–O(1)–Zn(1)	157.9(1)
V(1)–O(2)–V(1)#3	133.0(1)

Symmetry transformations used to generate equivalent atoms: #1 $-x+1, -y+1, z$. #2 $-x+1/2, -y+1, z-1/2$. #3 $-x+1/2, -y+1, z+1/2$.

Table 3 Selected bond lengths [Å] and angles [°] for $[Zn_3(tpyrtrz)_2(H_2O)_2V_6O_{18}]\cdot 6H_2O$ (**2**·$6H_2O$)

Zn(1)–O(2)#1	2.100(2)	V(1)–O(6)	1.651(3)
Zn(1)–O(2)	2.100(2)	V(1)–O(9)#2	1.801(2)
Zn(1)–N(1)#1	2.113(2)	V(1)–O(4)	1.810(3)
Zn(1)–N(1)	2.113(2)	V(2)–O(2)	1.635(2)
Zn(1)–O(1)	2.144(2)	V(2)–O(7)	1.660(2)
Zn(1)–O(1)#1	2.144(2)	V(2)–O(4)	1.744(2)
Zn(2)–O(7)	1.910(2)	V(2)–O(3)	1.772(2)
Zn(2)–O(8)	1.942(2)	V(3)–O(10)	1.614(3)
Zn(2)–N(5)	2.007(2)	V(3)–O(8)	1.684(2)
Zn(2)–N(6)	2.017(2)	V(3)–O(9)	1.761(3)
V(1)–O(5)	1.619(3)	V(3)–O(3)#3	1.800(3)
O(2)#1–Zn(1)–O(2)	180.0	O(6)–V(1)–O(9)#2	113.2(1)
O(2)#1–Zn(1)–N(1)#1	90.99(8)	O(5)–V(1)–O(4)	110.0(2)
O(2)–Zn(1)–N(1)#1	89.01(8)	O(6)–V(1)–O(4)	108.8(1)
O(2)#1–Zn(1)–N(1)	89.01(8)	O(9)#2–V(1)–O(4)	105.9(1)
O(2)–Zn(1)–N(1)	90.99(8)	O(2)–V(2)–O(7)	108.7(1)
N(1)#1–Zn(1)–N(1)	180.0(1)	O(2)–V(2)–O(4)	108.9(1)
O(2)#1–Zn(1)–O(1)	94.45(8)	O(7)–V(2)–O(4)	110.8(1)
O(2)–Zn(1)–O(1)	85.55(8)	O(2)–V(2)–O(3)	111.8(1)
N(1)#1–Zn(1)–O(1)	89.36(9)	O(7)–V(2)–O(3)	109.1(1)
N(1)–Zn(1)–O(1)	90.64(9)	O(4)–V(2)–O(3)	107.6(1)
O(2)#1–Zn(1)–O(1)#1	85.55(8)	O(10)–V(3)–O(8)	108.8(1)
O(2)–Zn(1)–O(1)#1	94.45(8)	O(10)–V(3)–O(9)	110.2(2)
N(1)#1–Zn(1)–O(1)#1	90.64(9)	O(8)–V(3)–O(9)	111.5(1)
N(1)–Zn(1)–O(1)#1	89.36(9)	O(10)–V(3)–O(3)#3	109.4(1)
O(1)–Zn(1)–O(1)#1	180.0(1)	O(8)–V(3)–O(3)#3	107.5(1)
O(7)–Zn(2)–O(8)	106.8(1)	O(9)–V(3)–O(3)#3	109.3(1)
O(7)–Zn(2)–N(5)	110.8(1)	V(2)–O(2)–Zn(1)	141.2(1)
O(8)–Zn(2)–N(5)	101.7(1)	V(2)–O(3)–V(3)#4	134.8(1)
O(7)–Zn(2)–N(6)	105.4(1)	V(2)–O(4)–V(1)	146.3(2)
O(8)–Zn(2)–N(6)	111.26(9)	V(2)–O(7)–Zn(2)	161.2(2)
N(5)–Zn(2)–N(6)	120.4(1)	V(3)–O(8)–Zn(2)	128.6(1)
O(5)–V(1)–O(6)	109.1(2)	V(3)–O(9)–V(1)#5	134.8(2)
O(5)–V(1)–O(9)#2	109.8(2)		

Symmetry transformations used to generate equivalent atoms: #1 $-x+2, -y+1, -z$. #2 $x-1, -y+1/2, z-1/2$. #3 $x, -y+1/2, z+1/2$. #4 $x, -y+1/2, z-1/2$. #5 $x+1, -y+1/2, z+1/2$. #6 $-x+2, -y+1, -z+1$.

tetrahedral vertex is defined by a terminal oxo-group directed into the interlamellar region. The terminal oxo-groups alternate up–down along the chain with respect to the $\{ZnV_2O_6\}$ plane.

The tetrahedral geometry at the Zn(II) sites is defined by two oxo-groups from adjacent vanadate chains and two pyridyl nitrogens, one from each of two monodentate tpytrz ligands, disposed above and below the metal oxide plane.

As demonstrated in Fig. 1a, only one pyridyl group of each tpytrz coordinates to a metal site, leaving two pendant groups projecting into the interlamellar region. Adjacent layers stack so as to produce a zipper mode of interdigitation of tpytrz groups. The monodentate coordination mode of the tpytrz is unanticipated since in the molybdate series the ligand behaved in all cases as a dipodal tether between adjacent layers. Consequently, the molybdate family exhibited three-dimensional connectivity, while **1** is a two-dimensional phase. The need to accommodate interdigitated sets of tpytrz units in the interlamellar region results in an oxide layer separation of 19.1 Å in **1**, in contrast to a spacing of 13.7 Å in $[Zn(tpytrz)_2Mo_4O_{13}]$.

A curious feature of the crystallography of **1** is the unusually long *b* axial length of 81.248(6) Å. However, careful examination of the structure reveals that the vanadate chains describe a shallow spiral and that chains from adjacent layers require five layer repeats to regain registry (Fig. 1a). Consequently, the axial length is a reflection of the asymmetry of the stacking of layers of entrained spiral chains.

Vanadate chains are common building blocks in secondary metal–ligand vanadium oxides.[37,38] The one-dimensional structures of the type $[Cu(ligand)V_2O_6]$ consists of chains of corner-sharing $\{VO_4\}$ tetrahedra decorated with $\{Cu(ligand)\}^{2+}$ subunits.[39–42] Such simple vanadate chains also provide building blocks for the two-dimensional structures $[Cu(en)V_2O_6]$,[39] β-$[Cu(terpy)V_2O_6]$[43] and $[Co(Hdpa)_2V_4O_{12}]$ (Hdpa = protonated dipyridylamine).[44] While two other examples of two-dimensional zinc–vanadates have been reported, the vanadate substructure of $[\{Zn(bpy)\}_2V_6O_{17}]$ is a two-dimensional network of corner-sharing tetrahedra and that of $[\{Zn(terpy)\}_2V_6O_{17}]$ consists of chains of $\{V_6O_{18}\}^{6-}$ rings.[43]

In contrast to the network structure of **1**, the architecture of $[Zn_3(tpytrz)_2(H_2O)_2V_6O_{18}]\cdot 6H_2O$ (**2**·$6H_2O$) is three-dimensional, as shown in Fig. 2. The framework is constructed from chains of corner-sharing vanadium tetrahedra, zinc tetrahedra $\{ZnN_2O_2\}$ and zinc octahedra $\{ZnN_2O_2(H_2O)_2\}$. The bimetallic oxide substructure itself is three-dimensional, providing large channels with profile dimensions in the *bc* plane of 11.6 × 11.3 Å which are occupied by the tpytrz ligands. This architecture exemplifies the construction of a material patterned after Scheme 2.

The structure may be described as ruffled networks of corner-sharing vanadium and zinc tetrahedra linked by zinc octahedra into a three-dimensional framework. As shown in Fig. 2b, the networks of zinc and vanadium tetrahedra in the *ac* plane are constructed from chains of corner-sharing $\{VO_4\}$ units linked by $\{ZnN_2O_2\}$ polyhedra, producing $\{Zn_2V_8O_{10}\}$ twenty-membered rings as the fundamental motif.

Each vanadate chain exhibits three distinct vanadium sites. One participates in corner-sharing to two neighboring vanadate tetrahedra, to one zinc tetrahedron in the layer and to the octahedral zinc site which serves to link layers. Consequently, this vanadium site possesses no terminal oxo-groups. The adjacent vanadate site contributes two corners to the chain and one corner to a tetrahedral zinc site of the layer, leaving one terminal oxo-group. The third vanadium site participates in corner-sharing to two adjacent vanadium centers of the chain and exhibits two-terminal oxo-groups.

The tetrahedral zinc site engages in corner-sharing with two vanadium sites of adjacent chains. The remaining coordination sites are occupied by pyridine nitrogens of two tpytrz ligands. The octahedral zinc site, which provides the connectivity between zinc vanadate layers, uses *trans* sites in corner-sharing to $\{VO_4\}$ tetrahedra from adjacent layers. The remaining coordination sites are occupied by nitrogen donors from two tpytrz ligands and two *trans* aqua ligands.

Table 4 Selected bond lengths [Å] and angles [°] for $[Cu_3(tpytrz)_2(H_2O)_2V_8O_{23}]\cdot 3H_2O$ (**3**·$3H_2O$)

Cu(1)–O(3)	1.963(3)	V(1)–O(7)#3	1.772(4)
Cu(1)–O(4)	1.965(3)	V(1)–O(1)	1.773(3)
Cu(1)–N(3)	1.983(4)	V(2)–O(5)	1.599(3)
Cu(1)–N(1)	2.010(4)	V(2)–O(4)	1.693(3)
Cu(1)–O(8)#1	2.496(4)	V(2)–O(1)#4	1.785(3)
Cu(1)–O(98)	2.644(7)	V(2)–O(6)	1.829(3)
Cu(2)–O(12)#2	1.940(4)	V(3)–O(8)	1.613(4)
Cu(2)–O(12)	1.940(4)	V(3)–O(7)	1.680(4)
Cu(2)–N(6)	1.956(4)	V(3)–O(6)	1.777(3)
Cu(2)–N(6)#2	1.956(4)	V(3)–O(9)	1.780(4)
Cu(2)–O(96)#2	2.49(1)	V(4)–O(11)	1.606(4)
Cu(2)–O(96)	2.49(1)	V(4)–O(12)	1.697(4)
V(1)–O(2)	1.635(4)	V(4)–O(10)	1.765(2)
V(1)–O(3)	1.710(4)	V(4)–O(9)	1.799(4)
O(3)–Cu(1)–O(4)	173.3(2)	O(12)#2–Cu(2)–N(6)#2	88.3(2)
O(3)–Cu(1)–N(3)	87.7(2)	O(12)–Cu(2)–N(6)#2	91.7(2)
O(4)–Cu(1)–N(3)	91.1(2)	N(6)–Cu(2)–N(6)#2	180.0(2)
O(3)–Cu(1)–N(1)	94.4(2)	O(12)#2–Cu(2)–O(96)#2	80.4(7)
O(4)–Cu(1)–N(1)	87.4(2)	O(12)–Cu(2)–O(96)#2	99.6(7)
N(3)–Cu(1)–N(1)	174.4(2)	N(6)–Cu(2)–O(96)#2	90.2(3)
O(3)–Cu(1)–O(8)#1	93.9(1)	N(6)#2–Cu(2)–O(96)#2	89.8(3)
O(4)–Cu(1)–O(8)#1	92.7(1)	O(12)#2–Cu(2)–O(96)	99.6(7)
N(3)–Cu(1)–O(8)#1	92.5(1)	O(12)–Cu(2)–O(96)	80.4(7)
N(1)–Cu(1)–O(8)#1	82.1(1)	N(6)–Cu(2)–O(96)	89.8(3)
O(3)–Cu(1)–O(98)	92.7(2)	N(6)#2–Cu(2)–O(96)	90.2(3)
O(4)–Cu(1)–O(98)	80.9(2)	O(96)#2–Cu(2)–O(96)	180.000(1)
N(3)–Cu(1)–O(98)	92.3(2)	O(2)–V(1)–O(3)	112.0(2)
N(1)–Cu(1)–O(98)	92.9(2)	O(2)–V(1)–O(7)#3	109.4(2)
O(8)#1–Cu(1)–O(98)	172.0(1)	O(3)–V(1)–O(7)#3	106.0(2)
O(12)#2–Cu(2)–O(12)	180.0(1)	O(2)–V(1)–O(1)	110.3(2)
O(12)#2–Cu(2)–N(6)	91.7(2)	O(3)–V(1)–O(1)	109.9(2)
O(12)–Cu(2)–N(6)	88.3(2)	O(7)#3–V(1)–O(1)	109.1(2)

Symmetry transformations used to generate equivalent atoms: #1 $-x + 3/2, -y + 1/2, z - 1/2$. #2 $-x + 1, -y, -z + 1$. #3 $-x + 1, y, -z + 1/2$. #4 $-x + 3/2, -y + 1/2, z + 1/2$. #5 $-x + 1, y, -z + 3/2$. #6 $x, -y + 1, z - 1/2$. #7 $x, -y + 1, z + 1/2$. #8 $-x + 3/2, y + 1/2, z$. #9 $-x + 3/2, y - 1/2, z$. #10 $x + 1, -y, z - 1/2$. #11 $x - 1, -y, z + 1/2$.

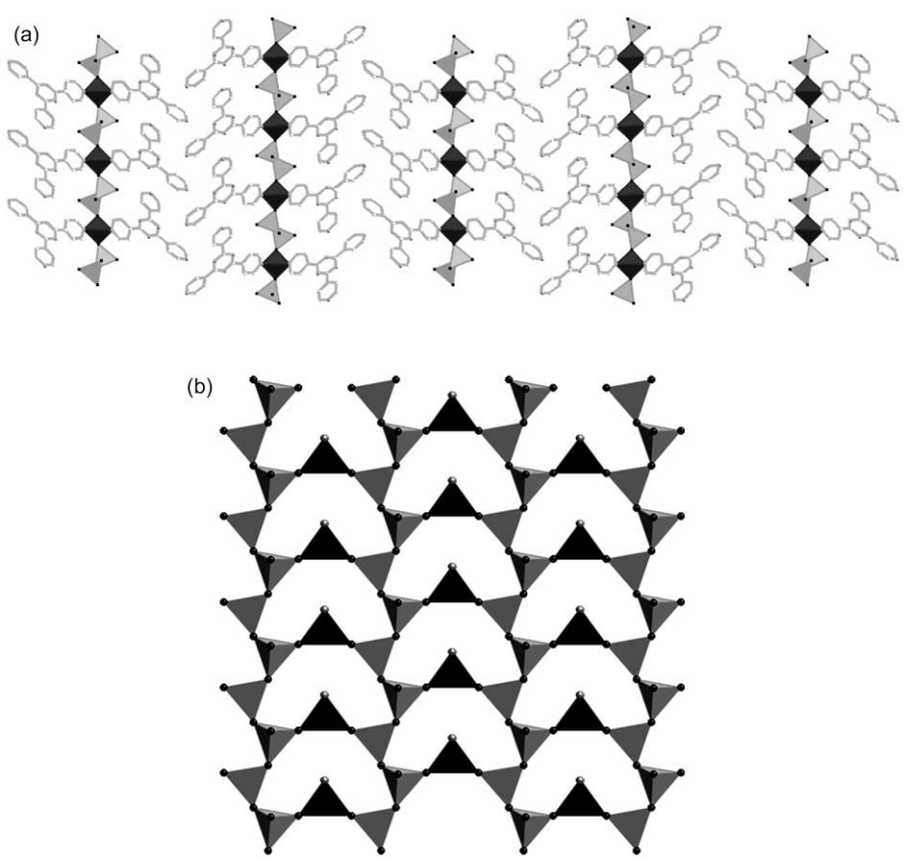

Fig. 1 (a) A polyhedral representation of the structure of $[Zn(tpytrz)_2V_2O_6]$ (**1**), viewed parallel to the *c* axis. The view reveals the need for five repeat units to bring the layers into registry. (b) A view of the $\{ZnV_2O_6\}$ bimetallic network. Scheme: zinc, dark polyhedra; vanadium, light polyhedra.

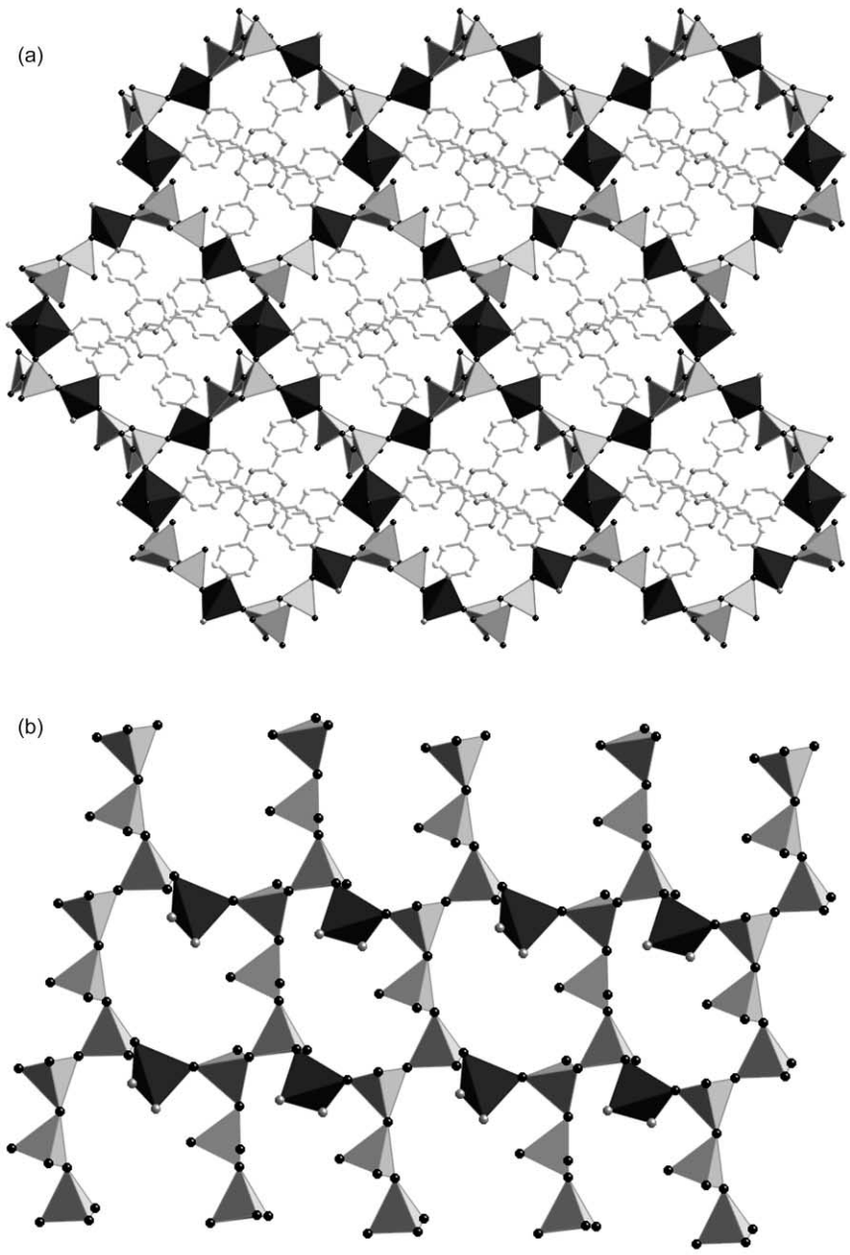

Fig. 2 (a) A polyhedral view of the three-dimensional structure of $[Zn_3(tpytrz)_2V_6O_{18}]$ (**2**), viewed parallel to the *a* axis and showing the large channels occupied by the tpytrz ligands. (b) The $\{Zn_2V_6O_{18}\}^{2n-}_{n}$ network of **2**, viewed parallel to the *b* axis.

Each tpytrz ligand bridges two tetrahedral zinc sites from adjacent layers and one octahedral Zn site. The channels occupied by these organic subunits are defined by rings of sixteen polyhedra $\{Zn_6V_{10}O_{16}\}$: two zinc octahedra, four zinc tetrahedra and ten vanadium tetrahedra. The water molecules of crystallization are located within these larger channels and within the smaller rings associated with the layers shown in Fig. 2b.

The three-dimensional structure of $[Cu_3(tpytrz)_2(H_2O)_2V_8O_{23}]\cdot 3H_2O$ (**3**·$3H_2O$), shown in Fig. 3, illustrates the consequences of substitution of Cu(II) for Zn(II) as the secondary metal component. Whereas Zn(II), a d^{10} cation, possess no crystal field imposed polyhedral preference and may consequently adopt tetrahedral, trigonal bipyramidal and octahedral geometries upon incorporation into a bimetallic oxide phase, Cu(II) generally adopts Jahn–Teller distorted '4 + 1' or '4 + 2' geometries. Consequently, while the architectural profile of **3** in the *ab* plane shows some similarities to that of **2**, the structural details of **3** are dramatically different from those observed for **2**.

The view of the structure of **3** parallel to the *c* axis illustrates that the overall architecture, in similar fashion to that of **2**, consists of a bimetallic oxide framework with the tpytrz components entrained in channels of dimensions 10.2 × 9.9 Å. However, despite this gross similarity in the overall structures of **2** and **3**, the detailed connectivity patterns and building blocks are quite distinct.

As shown in Fig. 3b, the vanadium oxide substructure consists of ruffled layers of corner-sharing $\{VO_4\}$ tetrahedra parallel to the *ac* plane, in contrast to the one-dimensional chains encountered for **2**. The connectivity of vanadate tetrahedra results in eighteen polyhedra or thirty-six membered rings $\{V_{18}O_{18}\}$. Each ring accommodates two Cu(II) sites. These Cu(1) sites exhibit '4 + 2' distorted octahedral geometry $\{CuO_3N_2(H_2O)\}$, defined by edge-sharing oxo-groups from three vanadate tetrahedra, *trans* oriented pyridyl donors from two tpytrz ligands and an aqua ligand which projects into the intralamellar cavity provided by the ring.

The Cu(2) sites occupy the top and bottom surfaces of this vanadate layer and serve to connect adjacent layers into the overall three-dimensional framework. This Cu(II) site exhibits $\{CuO_2N_2(H_2O)_2\}$ '4 + 2' geometry, through *trans* edge-sharing with oxo-groups of $\{VO_4\}$ units from adjacent

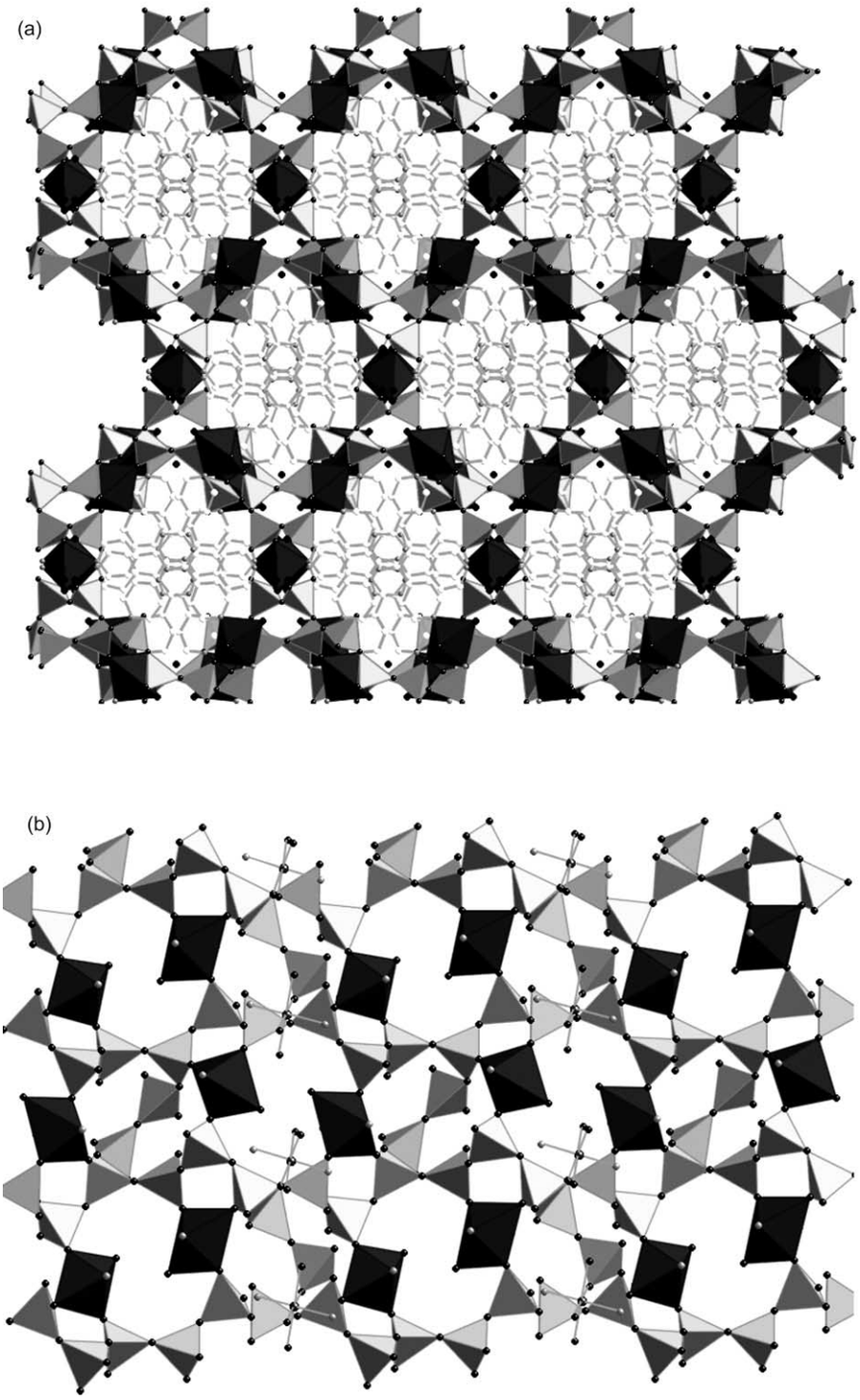

Fig. 3 (a) A polyhedral representation of the three-dimensional structure of $[Cu_3(tpytrz)_2V_8O_{23}]$ (**3**), viewed parallel to the *c* axis. (b) A view of the vanadate network of **2** in the *ac* plane. The polyhedral Cu(II) sites lie in the plane, while the Cu(II) sites described in ball and stick representation project from the surfaces of the layer and link adjacent networks.

layers, *trans* bonding to pyridyl nitrogen donors from two tpytrz ligands and to two aqua ligands.

The $\{Cu_3(tpytrz)_2\}_n^{6n+}$ substructure is also two-dimensional. The linkage of tpytrz ligands and Cu(II) sites generates a slab three polyhedra thick. Each tpytrz links two Cu(1) sites and one Cu(2) site while occupying a cavity generated by a twenty polyhedra connect or forty-membered double loop $\{Cu_2V_{18}O_{20}\}$.

Thermal behavior

The thermal characteristics of **1**–**3** reflect their unique structural characteristics. The thermal decomposition of **1** exhibits a weight loss of *ca.* 18% between 320 and 360 °C, consistent with the loss of a pendant pyridyl group. This conclusion is supported by elemental analysis of the products of heating **1** at 360 °C in dynamic vacuum for 2 h, which were consistent with the loss of a pyridyl unit. The thermal product of **1** is stable to 450 °C, whereupon a second weight loss of *ca.* 70% occurs, corresponding to the loss of the bipyridyltriazine ligand fragment. The resultant gray residue is amorphous.

The thermal decomposition of **2** exhibits dehydration in two steps in the temperature ranges 130–145 °C and 220–245 °C. The first step is associated with a weight loss of *ca.* 7%, consistent with release of three water molecules of crystallization, while the second dehydration corresponds to a weight loss of *ca.* 2%, associated with the release of the aqua ligands. Since

the mechanism of dehydration is dependent on topological and energetic considerations,[45] the more accessible and unbound water molecules of crystallization are expected to be released at significantly lower temperature than those coordinated to metal sites. The dehydration steps are followed by gradual release of the organic component, a weight loss of 40% over the range 360–450 °C.

The thermal behavior of **3**·3H_2O is similar to that of **2**·6H_2O. The loss of water of crystallization (*ca.* 3.2% weight loss) occurs at 138 °C, while the aqua ligands (2.0% weight loss) are released at *ca.* 230–255 °C. Ligand loss (37% weight loss) occurs between 370 and 460 °C.

The powder diffraction patters of dehydrated samples **2** and **3** are consistent with amorphous materials. However, exposure of **2** and **3** to H_2O for 12 h results in powder patterns identical to those of **2**·6H_2O and **3**·3H_2O, respectively. These observations suggest that the interior pore volumes of **2** and **3** are accessible. We are investigating the sorption properties of these materials with respect to polar organic solvents and various gas molecules.

Conclusions

The combination of hydrothermal methods and the use of organic components as structure-directing subunits in the construction of organic/inorganic hybrids provides a powerful strategy for the development of new materials. The architectures of these materials are profoundly influenced by the identity of the organic constituent. In the specific case of tripyridyltriazine (tpytrz) of this study, the ligand may adopt monodentate, bidentate or tridentate coordination modes, resulting in vastly different oxide microstructures. In the case of the previously reported molybdenum oxide phases of which [M′(tpytrz)$_2$Mo$_4$O$_{13}$] [M′ = Fe, Co, Ni, Zn] is representative, the ligand adopts a dipodal mode of attachment, thus favoring three-dimensional structures constructed from bimetallic oxide layers and ligand tethers. In contrast, the vanadium oxide system exhibits two-dimensional and three-dimensional architectures with dramatically different oxide substructures. The three-dimensional materials [Zn_3(tpytrz)$_2$(H_2O)$_2$$V_6O_{18}$]·6$H_2O$ (**2**·6H_2O) and [Cu_3(tpytrz)$_2$(H_2O)$_2$$V_8O_{23}$]·3$H_2O$ (**3**·3H_2O) exhibit the ligand in a tridentate coordination mode, entrained within channels formed by the bimetallic oxide frameworks which condense about the structure-directing organic moiety. The structurally distinct {$Zn_3V_6O_{18}$} and {$Cu_3V_8O_{23}$} oxide substructures reveal the influences of the coordination preferences of the secondary metal component and the subtle interplay of the constituents of this three component system: secondary metal, organic ligand, and vanadium oxide.

The hydrothermal method overcomes the limitation of being able to synthesize only the thermodynamic dense phases obtained by classical ceramic methods and provides an approach to the design of zeolites and other microporous solids, intercalation compounds, pillared layered materials and in our case inorganic–organic hybrid materials. The synthetic approach adopted for the evolution of these oxide hybrid materials draws on the fundamental principles of coordination chemistry in their design. The guiding principle in this strategy is that the information necessary for the design of the extended hybrid structures is present at the molecular level in the starting materials or component building blocks. Consequently the syntheses rely on self-assembly and borrow conceptually from the fields of supramolecular chemistry and "crystal engineering".[46] However, it is important to appreciate that the design principles inherent in this approach provide only a broad blueprint, relying often on serendipitous discovery of new architectures and the judicious selection of component substructures.[47] While the ability to rationally design materials for use in fundamental studies or practical applications motivates such synthetic studies, the complexity and range of interactions within most solids precludes accurate structural predictions. However, through the accumulation of a structural database for a particular family of materials, empirical rules can emerge to aid in the design and control of structure.

Acknowledgements

This work was supported by a grant from the National Science Foundation (CHE9987471).

References and notes

1 N. N. Greenwood and A. Earnshaw, *Chemistry of the Elements*, Pergamon Press, New York, 1984.
2 (*a*) W. Büchner, R. Schliebs, G. Winter and K. H. Büchel, *Industrial Inorganic Chemistry*, VCH, New York, 1989; (*b*) B. Cockayne and D. W. Jones, *Modern Oxide Materials*, ed. D. W. Jones, Academic Press, New York, 1972.
3 W. Büchner, R. Schliebs, G. Winter and K. H. Büchel, *Industrial Inorganic Chemistry*, VCH, New York, 1989.
4 W. H. McCarroll, *Encyclopedia of Inorganic Chemistry*, ed. R. B. King, John Wiley & Sons, New York, 1994, vol. 6, 2903.
5 G. M. Whitesides and R. F. Ismagilov, *Science*, 1999, **284**, 89.
6 J. M. Lehn, *Proc. Natl. Acad. Sci. USA*, 2002, **99**, 4763.
7 (*a*) S. I. Stupp and P. V. Braun, *Science*, 1997, **277**, 1242; (*b*) M. E. Davis, A. Katz and W. R. Ahmad, *Chem. Mater.*, 1996, **8**, 1820.
8 *Proceedings of the First European Workshop on Hybrid Organic–Inorganic Materials*, special issue of *New J. Chem.*, 1994, **18**, ed. C. Sanchez and F. Ribot.
9 P. J. Hagrman, D. Hagrman and J. Zubieta, *Angew. Chem., Int. Ed.*, 1999, **38**, 2638.
10 D. Hagrman, C. Zubieta, R. C. Haushalter and J. Zubieta, *Angew. Chem., Int. Ed. Engl.*, 1997, **36**, 873.
11 D. Hagrman, C. Sangregorio, C. J. O'Connor and J. Zubieta, *J. Chem. Soc., Dalton Trans.*, 1998, 3707.
12 D. Hagrman, P. Hagrman and J. Zubieta, *Inorg. Chim. Acta*, 2000, **300–302**, 212.
13 J. R. D. DeBord, R. C. Haushalter, L. M. Meyer, D. J. Rose, P. J. Zapf and J. Zubieta, *Inorg. Chim. Acta*, 1997, **256**, 165.
14 D. Hagrman, P. J. Zapf and J. Zubieta, *Chem. Commun.*, 1998, 1283.
15 D. Hagrman, P. J. Hagrman and J. Zubieta, *Angew. Chem., Int. Ed.*, 1999, **38**, 3165.
16 D. Hagrman and J. Zubieta, *C. R. Acad. Sci., Ser. IIc*, 2000, **3**, 231.
17 D. Hagrman, P. J. Hagrman and J. Zubieta, *Comments Inorg. Chem.*, 1999, **21**, 225 and references therein.
18 D. J. Chesnut, D. Hagrman, P. J. Zapf, R. P. Hammond, R. LaDuca, Jr., R. C. Haushalter and J. Zubieta, *Coord. Chem. Rev.*, 1999, **190–192**, 737.
19 P. J. Zapf, R. P. Hammond, R. C. Haushalter and J. Zubieta, *Chem. Mater.*, 1998, **10**, 1366.
20 D. Hagrman, C. J. Warren, R. C. Haushalter, C. Seip, C. J. O'Connor, R. S. Rarig, Jr., K. M. Johnson III, R. L. LaDuca, Jr. and J. Zubieta, *Chem. Mater.*, 1998, **10**, 3294.
21 D. Hagrman, R. C. Haushalter and J. Zubieta, *Chem. Mater.*, 1998, **10**, 361.
22 M. C. Laskoski, R. L. LaDuca, Jr., R. S. Rarig, Jr. and J. Zubieta, *J. Chem. Soc., Dalton Trans.*, 1999, 3467.
23 D. E. Hagrman and J. Zubieta, *J. Solid State Chem.*, 2000, **152**, 141.
24 R. L. LaDuca, Jr., M. Desciak, M. Laskoski, R. S. Rarig, Jr. and J. Zubieta, *J. Chem. Soc., Dalton Trans.*, 2000, 2255.
25 P. J. Zapf, C. J. Warren, R. C. Haushalter and J. Zubieta, *Chem. Commun.*, 1997, 1543.
26 R. S. Rarig and J. Zubieta, *J. Chem. Soc., Dalton Trans.*, 2001, 3446.
27 (*a*) A. Clearfield, *Prog, Inorg. Chem.*, 1998, **47**, 371; (*b*) D. M. Poojary, B. Zhang, P. Bellinghausen and A. Clearfield, *Inorg. Chem.*, 1996, **35**, 5254; (*c*) G. Huan, A. J. Jacobson, J. W. Johnson and E. W. Corcoran, Jr., *Chem. Mater.*, 1990, **2**, 91.
28 D. B. Mitzi, *J. Chem. Soc., Dalton Trans.*, 2001, 1.
29 H. G. Biedermann and K. Wichmann, *Z. Naturforsch., Teil B*, 1974, **296**, 360.
30 SMART, Data Collection Software, version 4.050, Siemens Analytical Instruments Inc., Madison, WI, 1996.
31 SAINT, Data Reduction Software, version 4.050, Siemens Analytical Instruments Inc., Madison, WI, 1996.
32 G. M Sheldrick, SADABS, University of Göttingen, Germany, 1996.
33 SHELXTL PC, Siemens Analytical X-Ray Instruments Inc., Madison, WI, 1993.

34 R. A. Laudise, *Chem. Eng. News*, 1987, **65**, 30.
35 A. N. Lobachev, *Crystallization Processes Under Hydrothermal Conditions*, Consultants Bureau, New York, 1973.
36 J. Gopalakrishnan, *Chem. Mater.*, 1995, **7**, 1265.
37 P. J. Hagrman, R. C. Finn and J. Zubieta, *Solid State Sci.*, 2001, **3**, 745.
38 P. Y. Zavalij and M. S. Whittingham, *Acta Crystallogr., Sect. B*, 1999, **1355**, 627.
39 J. R. D. DeBord, Y. Zhang, R. C. Haushalter, J. Zubieta and C. J. O'Connor, *J. Solid State Chem.*, 1996, **122**, 251.
40 R. C. Finn and J. Zubieta, unpublished results.
41 B.-Z. Lin and S.-X. Liu, *Polyhedron*, 2000, **19**, 2521.
42 L.-M. Zheng, J.-S. Zhao, K.-H. Lii, L.-Y. Zhang, Y. Liu and X.-Q. Xin, *J. Chem. Soc., Dalton Trans.*, 1999, 939.
43 P. J. Hagrman and J. Zubieta, *Inorg. Chem.*, 2000, **39**, 3252.
44 R. L. LaDuca, R. S. Rarig and J. Zubieta, *Inorg. Chem.*, 2001, **40**, 607.
45 S. Petit and G. Coquerel, *Chem. Mater.*, 1996, **8**, 2247.
46 "Crystal engineering" is here used in the broadest sense of modification of the extended structure of a material. The organic components in the hybrid materials of this study allow isolation of bimetallic oxide chains which are otherwise inaccessible in M(II)/V/O solid state chemistry.
47 M. J. Zaworotko, *Chem. Commun.*, 2001, 1.